LAWRENCE
LIVERMORE
NATIONAL
LABORATORY

LLNL-CONF-656786

NON-DISPERSIVE RESPONSE OF A HOPKINSON BAR TO SHOCK LOADING

D. W. Baum

July 8, 2014

DYMAT Hopkinson Centenary Conference
Cambridge, United Kingdom
September 9, 2014 through September 11, 2014

Disclaimer

Non-Dispersive Response of a Hopkinson Bar to Shock Loading

Dennis W. Baum
Lawrence Livermore National Laboratory

1 Abstract

This paper is intended to draw attention to a unique aspect of the Hopkinson bar, which while not new, has not been exploited by the blast wave measurement community. The nearly 50-year-old work referenced herein established a solid theoretical basis for realizing a highly resolved temporal measurement of blast wave pressure profiles. The referenced work also compares the calculated bar response with shock tube experiments producing a step-function loading profile on a bar, mounted internal to and co-axial with the shock tube. Within the fidelity of the instrumentation and recording equipment, the experiments verified both the qualitative and quantitative analytical analysis of bar response. This paper respectfully revisits prior work on this centenary occasion as a fulfillment of the original intent of Hopkinson to measure blast waves and impactor effects.

2 Introduction

For the last 100 years and up to the present day, the Hopkinson bar technique[1] has been an important laboratory tool to study the response of materials to dynamic loads. In practice, the Hopkinson bar technique has been applied primarily in the moderate strain rate regime, rather than for the measurement of blast and impactor effects as envisioned by Hopkinson. Three fundamental papers provide the theoretical foundation for the response of a bar to dynamic loading and thus are key to understanding the limitations and therefore applications of a Hopkinson bar.

The first two are the early theoretical work of Pochhammer[2] and Chree[3] that proved that sinusoidal waves traveling in an infinite bar with a condition of zero stress at the lateral surface leads to an equation connecting phase velocity and frequency of the waves. This conclusion is important because this phase velocity and frequency relationship requires that a pulse, which

can be described in the frequency domain as a composition of Pochhammer-Chree (PC) waves of many frequencies, would be expected to change shape during travel. This inherent dispersive nature of wave propagation in a bar presents a fundamental limitation on the frequency response of a bar and thus limits its utility to moderate frequencies pulses and strain rates. A third paper by Folk, Fox, Shook, and Curtis[4] examined the common end-loading usage of a bar and provided an exact solution to the problem of calculating the strain due to time-dependent end-loading of a semi-infinite bar. This work concerned calculating the amplitude of the resulting oscillations in the bar, the relative importance of the various possible modes of vibration, and the dependence of pulse shape on the conditions of loading. A method was presented for calculating the elastic strain produced by the sudden application of pressure to the end of a semi-infinite cylindrical bar with a stress-free lateral surface. The exact solution is expressed as a sum of Fourier integrals whose integrands have the form of Pochhammer–Chree waves, which can be evaluated to obtain asymptotic solutions valid at large distances from the end of the bar. These solutions take the form of an Airy[5] function, shown in Fig. 1, which is a wave form consisting of a low frequency rise followed by a series of higher frequency waves of diminishing amplitude and increasing frequency. These findings explain the limitation of the Hopkinson bar to response regimes of moderate strain rates.

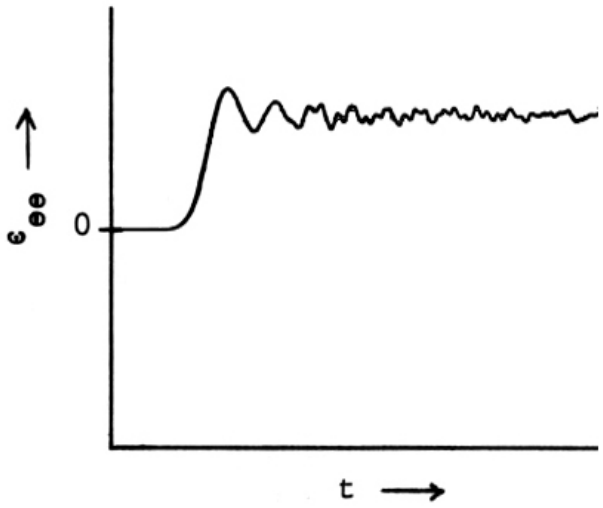

Fig. 1. Strain observed on surface of a cylindrical bar subject to step-function end-loading [ref. 4].

The “current” 50-year-old referenced work by Baum[5] builds on these prior papers and uses the same theoretical approach for calculating the time-dependent response of a bar subject to a traveling lateral surface load.

Within the same asymptotic solution conditions, there is found an additional non-dispersive term in addition to the Pochhammer-Chree waves. This additional finding enables a high-fidelity time-resolved response of a bar to a time-varying load.

This paper reviews the approach to the analysis described in Ref. 5 and the significant results, but refers back to Ref. 5 for detailed descriptions of the analysis. Copies of the original data records from the Baum thesis[6], which verify the analysis, are contained herein and suggest the potential utilization of the Hopkinson bar for high resolution blast wave and shock tube pressure measurements. The included figures are referenced to their original sources.

3 Description of Analytic Problem

3.1 Lateral Surface Loading

The problem to be solved is the determination of the elastic strain in a cylindrical bar of radius a, subject to a step function in stress, τ_{rr}, traveling at velocity V, applied normal to the lateral surface, and subject to zero stress, $\tau_{zz,}$ and radial displacement, $\mu_{r,}$ on the end of the bar. These boundary conditions are illustrated in Fig. 2.

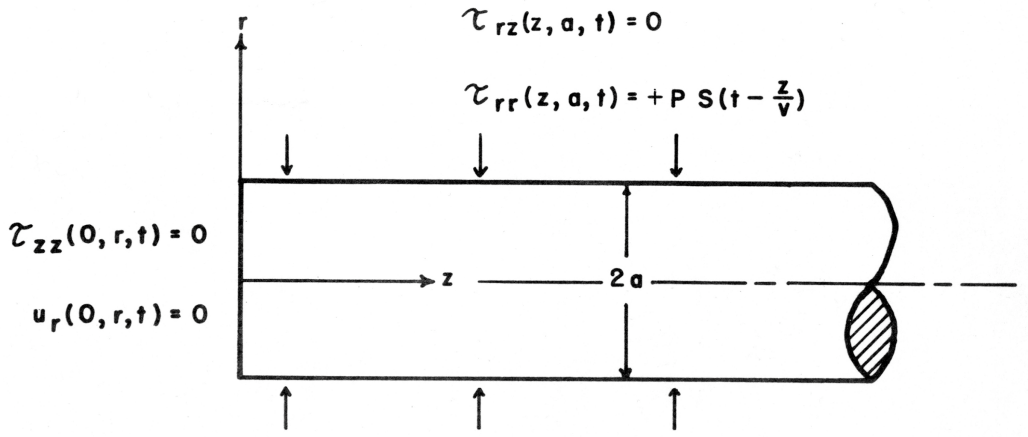

Fig. 2. Boundary conditions for constant velocity normal stress loading on the lateral surface of a bar [ref. 5].

This is a mixed-end condition problem (one component of stress and one component of displacement, specified on the end of the bar). The end

conditions chosen allow the use of the double transform method of solution presented by Folk et al. The assumption regarding the value of the end displacement is relatively unimportant for strains at large distances from the end of the bar and serves to enable the solution technique.

The equations of motion for a bar having cylindrical symmetry and the coordinates as shown in Fig. 2 are:

$$\rho \frac{\partial^2 u_r}{\partial t^2} = (\lambda + 2\mu) \frac{\partial \Delta}{\partial r} + 2\mu \frac{\partial \Omega}{\partial z} \tag{1}$$

$$\rho \frac{\partial^2 u_z}{\partial t^2} = (\lambda + 2\mu) \frac{\partial \Delta}{\partial z} - \frac{2\mu}{r} \frac{\partial (\mathrm{r}\Omega)}{\partial r} \tag{2}$$

$$\Delta = \frac{1}{r} \frac{\partial (r u_r)}{\partial r} + \frac{\partial u_z}{\partial z} \tag{3}$$

$$\Omega = \frac{1}{2} \left(\frac{\partial u_r}{\partial z} - \frac{\partial u_z}{\partial r} \right) \tag{4}$$

In these equations t is time, u_r and u_z are radial and axial displacements respectively, ρ is the density and λ and μ are the Lamé elastic constants. Δ and Ω are defined by equations (3) and (4).

Solutions to these equations must satisfy the following initial and boundary conditions:

(a) the initial conditions at $t = 0$,

$$u_r = u_z = \frac{\partial u_r}{\partial t} = \frac{\partial u_z}{\partial t} = 0 \tag{5}$$

(b) the boundary conditions on the lateral surface, r = a,

$$\begin{aligned} \tau_{rr}(z, a, t) &= PS\left(t - \frac{z}{v}\right) \\ \tau_{rz}(z, a, t) &= 0 \end{aligned} \tag{6}$$

(c) the boundary conditions at the end of the bar,
z = 0,

$$\tau_{zz}(o,r,t) = 0$$
$$u_r(o,r,t) = 0 \tag{7}$$

P represents the amplitude of the applied normal stress, V is the loading velocity, and $S\left(t - \frac{z}{\nu}\right)$ is a step function in time moving at speed V. In addition, the stress components τ_{rr}, τ_{rz}, and τ_{zz} are related to the displacements by the stress-strain equations.

$$\tau_{zz} = \frac{\lambda}{r}\frac{\partial(ru_r)}{\partial r} + (\lambda + 2\mu)\frac{\partial u_z}{\partial z} \tag{8}$$

$$\tau_{rr} = (\lambda + 2\mu)\frac{\partial u_r}{\partial r} + \frac{\lambda u_r}{r} + \lambda\frac{\partial u_z}{\partial z} \tag{9}$$

$$\tau_{rz} = \mu\left(\frac{\partial u_r}{\partial z} + \frac{\partial u_z}{\partial r}\right) \tag{10}$$

Equations (1) through (10) completely specify the problem.

Asymptotic solutions to the equations of motion valid at a long distance from the loaded end of the bar were obtained. These solutions predict time-dependent strain, which may be described as the superposition of several waves each of which propagates with a characteristic velocity. The strain produced by a positive normal loading of the lateral surface consists of a radial expansion followed by a radial compression. The initial radial expansion has the form of an Airy function and propagates at the bar velocity $C_o = \sqrt{Y/\rho}$. This wave is dispersive and its amplitude is a function of V, the elastic constants for the bar material, and the normal stress P. It is analogous to the pulse emanating from end-loading of the bar. The subsequent radial compression pulse is non-dispersive and can have several components traveling at the surface loading velocity and is best understood from the Pochhammer-Chree solutions in the Ω, Γ plane, where $\Omega = \omega/C_s$ and $\Gamma = \Upsilon a$, where the shear wave velocity $C_s = (\mu/\rho)^{1/2}$, as shown in Fig. 3.

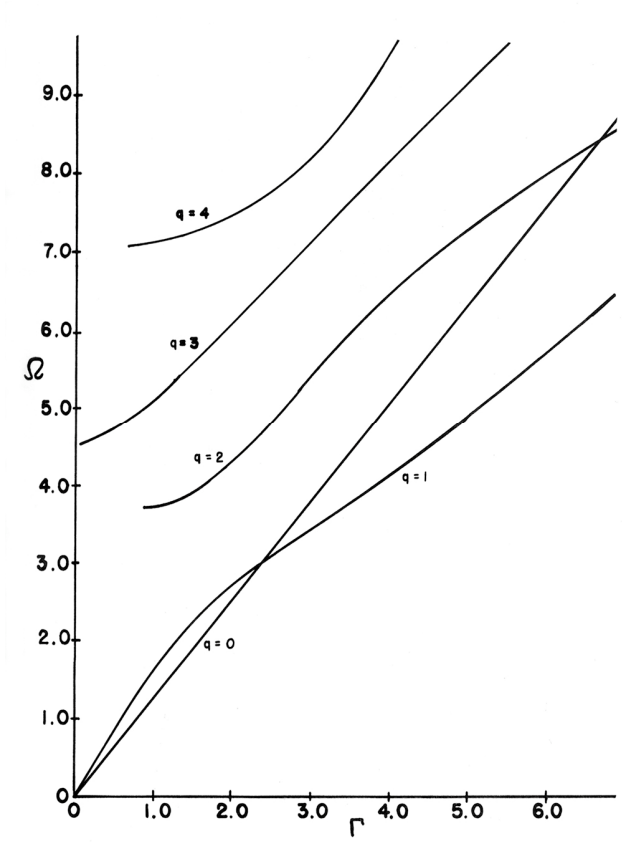

Fig. 3. Pochhammer-Chree dispersion curves for a bar having a Poisson's ratio of σ = 0.35 [ref. 4].

The curves in Fig. 3 having mode q>0 represent allowable propagation frequencies and wave speeds according to PC, expressed in terms of elastic bar properties. The slope of the curves at any given point describes the propagation velocity of waves at the corresponding frequency. Thus, it can be readily seen that there are discrete relationships between wave propagation speed and wave frequency. With end-loading of the bar, the PC curves for q>0 prescribe the only allowable propagation speeds of elastic waves of a given frequency. The result of this dispersive frequency propagation speed relationship prescribes the pulse shape in Fig. 1, where low frequency waves at the head of the pulse are traveling faster than the high frequency waves, which arrive later in time.

Of particular significance in this paper is the additional zeroth mode, q=0, resulting from the lateral surface loading and is a straight line indicating that particular mode allows propagation of all frequencies at the same speed, which corresponds to the surface loading speed V, i.e., it is a non-dispersive mode. Note that its slope (propagation speed) is directly proportional to the

loading velocity, whereas all the higher PC modes are dependent only on bar parameters. For a given bar material and size, along with an assumed loading speed and pressure amplitude, the compressive bar response to step-function compressive loading has been calculated.[5] An understanding of Fig. 2 provides a description of the response of a bar to both end-loading and lateral surface loading.

For all modes higher than the first (q>1), the phase velocity in the high frequency limit is the shear velocity C_s. The high frequency limit phase velocity of the first mode (q=1) is the Rayleigh surface wave velocity. The minimum phase velocity of the first mode C_{min}, is only slightly less than the Rayleigh velocity.

For loading velocities less than C_{min}, (roughly three-fourths of the elastic shear wave velocity C_s) the zeroth mode line does not intersect any PC mode curves and so wave propagation speed is constant at the loading speed V, for all wave frequencies. This zeroth mode result allows, in theory, a bar to respond to a lateral loading pulse with exquisitely faithful reproduction of the loading pulse. Of course limitations will arise from the finite dimensions of sensors employed to detect bar response, which will be discussed later.

For all loading velocities greater than or equal to C_{min}, there is at least one intersection of the zeroth mode and one or more of the PC modes. The intersection of the zeroth mode and a higher order mode will result in the zeroth mode non-dispersive response, followed by the singular frequency wave corresponding to the higher order PC mode intersect point.

3.2 Shear Stress Loading

An additional loading condition on the lateral surface of the bar is associated with a gas dynamic shock wave loading. The boundary layer flow behind a shock wave propagating along the lateral surface of a cylindrical bar exerts a shear stress on the surface of the bar. In order to establish the qualitative nature of the resulting strain, the equations of motion, Eqs. 1-4, were again solved using the method of Folk et al. The same initial conditions and end conditions were used, but the boundary conditions on the lateral surface were assumed to be zero radial stress and a step-function shear stress traveling at the loading speed V. In reality, the shear stress should decrease with distance behind the shock, but as our intent here is only to understand

the character of shear stress loading on bar response, the shear stress was assumed constant behind the shock.

The results of the double transform inversion technique predict that at time $t = z/C_o$, a positive shear stress produces a strain, which rises linearly with time. With the arrival of the loading shock at $t = z/V$ a linearly decreasing strain is added to the first so that the total shear strain decrease linearly with time.

3.3 Mathematical Summary

Figure 4 illustrates bar response to lateral surface loads of two different speeds. Note that for all loading speeds there is an initial Airy function expansion pulse traveling down the bar at the bar velocity C_o, followed by a compression load associated with and traveling at the loading speed V. The final strain in the bar is the sum of these two pulses and reduces to the static solution for radial compressive strain = $(P/E)(1-\sigma)$ and is independent of loading speed.

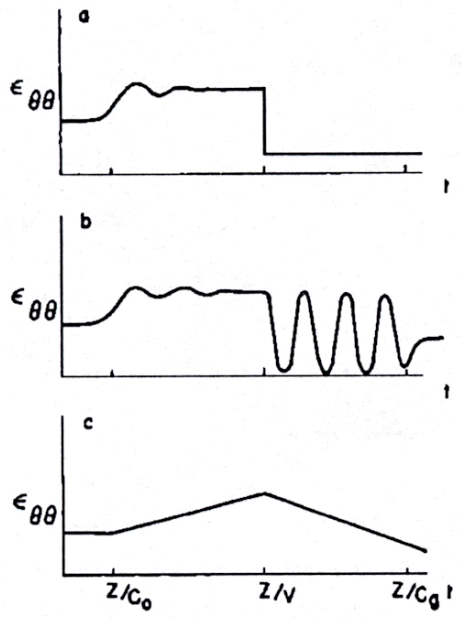

Fig. 4. Circumferential strain time profiles for a bar. (a) Normal stress loading, $V<C_{min}$; (b) normal stress loading, $C_{min}<V<C_o$; (c) shear stress loading, $V< C_{min}$ [ref. 5].

For $V < C_{min}$, total circumferential strain consists of an Airy function strain signal propagating in the bar with the bar velocity C_o followed by a negative step strain propagating with the loading velocity V, as shown in Fig. 4(a).

For $C_o > V > C_{min}$, circumferential strain consists of the Airy function strain signal and the negative step strain of the previous case. The sinusoidal oscillations predicted by the intersection of the zeroth and first mode of the PC curves begin immediately following the negative step strain and continue until arrival of similar oscillations traveling with the group velocity. These two oscillations have the same frequency but are out of phase so they cancel exactly as shown in Fig. 4(b), and the strain in the bar is at its equilibrium value under the load P. The circumferential strain induced in a cylindrical bar by a transient shear step stress traveling with the shock speed consists of a linearly increasing ramp, which arrives at a time $t = z/C_o$, followed by a linearly decreasing ramp, which begins at a time $t = z/V$, as shown in Fig. 4(c).

An additional phenomenon not considered here is the thermal loading of the bar, which can further complicate bar and gage response intended solely to measure pressure induced circumferential strain.

4 Experimental Configuration

The experiment designed to verify the preceding predictions for time-dependent strain in a bar required: A normal step-function stress loading of constant magnitude and loading velocity, strain measurements on a time scale allowing convenient comparison with the predictions, and use of a bar of sufficient length to allow completion of strain measurements before the arrival of strain waves reflected from the downstream end of the bar.

A conventional constant diameter bursting diaphragm shock tube, which had a 3.8cm diameter by 1.5m long driver section and a 7.0m driven section, was used to produce a well characterized step-function loading pulse of shocked air. The driver section was pressurized with helium (2,000-lb/in.^{2} maximum), and produced shock waves of desired speed and magnitude in the driven section. The shock velocity V was determined by recording the shock transit time between a pair of glow-discharge gages, placed 86 cm apart. Shock velocities were believed accurate to ±2%. Shock pressure was computed from normal shock tables using the measured values of V, the initial pressure and temperature of the air in the driven section. The resulting shock pressure

jump –P loading the bar were believed accurate to ±3%. The loading pressure ranged from 0.2 bar for fast shocks to 2.5 bar for slow shocks.

The driven section of the shock tube was modified to accommodate a long instrumented bar, co-axial with the shock tube, allowing the shocked air to establish an annular flow that progressively enveloped the lateral surface of the bar. The Plexiglas measuring bar was 0.95cm in diameter and 2.9m long. Plexiglas was chosen because its relatively low Young's modulus produces a larger strain than common metals such as Al or steel. A complication associated with the use of Plexiglas is its visco-elastic behavior, which was observed in the experiments. To aid in the development of a smooth region of annular flow along the bar, a lead-in bar of the same diameter and 350cm long was mounted upstream of the instrumented bar. A second but important role of the lead-in bar was to eliminate a reflected shock end-loading of the instrumented bar. To accomplish these goals, a small gap was adjusted between bars allowing the shocked gas to rapidly fill and equilibrate to the shocked gas pressure. A gap of <2mm was found to accomplish both purposes. The Plexiglas bar has a low bar velocity, C_0=2.08 km/sec, compared with metals, and its length allows an observation time of more than 2 msec before arrival of elastic waves reflected from the end of the bar. The low C_o also allows the bar to be studied over a broad range of loading velocities relative to the PC response modes portrayed and discussed in Fig. 3. Fine copper wires spaced at 90 cm intervals supported the bars and were adjustable to center the bars coaxial with the shock tube. No support was within 30 cm of either strain gage and no effect of the supports was observed on the experimental records.

A schematic of the shock tube, bar assembly, and instrumentation is shown in Fig. 5.

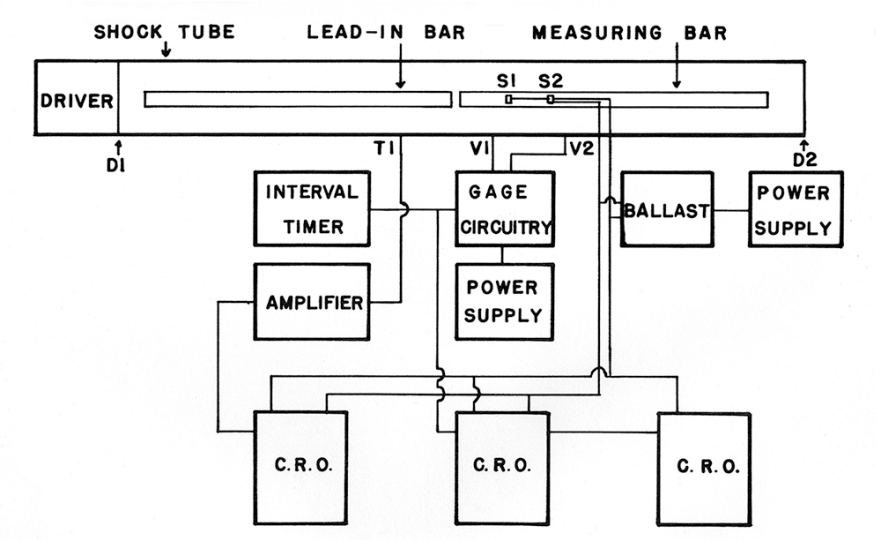

Fig. 5. Block diagram of the experiment setup [ref. 6].

V1 and V2 were glow discharge gages used to measure the average shock speed along the instrumented section of the bar. S1 and S2 are strain gages embedded beneath the surface of the bar to measure circumferential strain of the bar while being isolated from direct contact with the shocked gas. The gages were 30 cm apart. Gages S1 and S2 each consisted of four thin-film metal strain gages connected in series and placed symmetrically on the measuring bar. This arrangement provided negligible sensitivity to flexural waves while providing maximum sensitivity to circumferential strain. A constant 10.0 mA current powered the gages and a gage voltage change of 0.3 mV resulted from a typical shock-produced strain of 10^{-5}. Shock transit times across the 0.185cm width of the strain gages ranged between 1 and 3 μsec in these experiments. The signals were recorded on Tektronix type 555 and 585 oscilloscopes equipped with type D amplifiers.

Figures 6 and 7 are data records of circumferential strain vs time representative of different regimes of shock velocities studied. Strain is positive upward and time progresses from left to right.

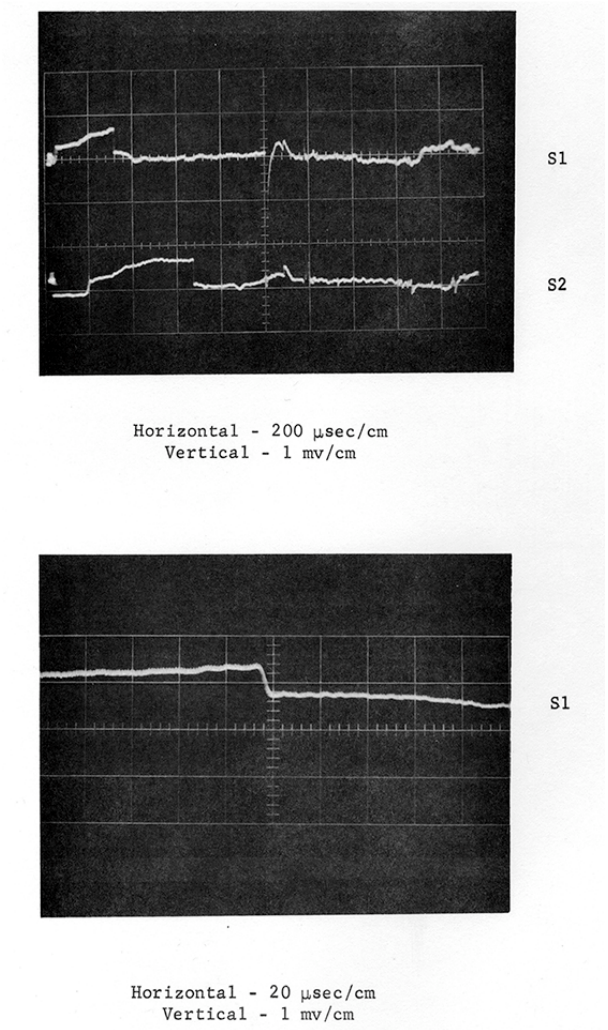

Fig. 6. S1 and S2 strain gage records for shock velocity $V=0.877 \times 10^5$ cm/sec [ref. 6].

Figure 6 shows a representative data record of S1 and S2 strain gage voltages versus time. Increases in strain are positive on the vertical axis and time increases from left to right. The shock velocity ($V=0.877 \times 10^5$cm/sec) is less than the minimum phase velocity of the first PC mode ($C_{min}=1.184 \times 10^5$ cm/sec). The first signal on the left travels with the bar velocity C_o and is produced both by the loading of the lateral surface and by the filling of the gap between the lead-in and measuring bars. The slowly rising ramp signal has the qualitative features predicted for shear loading on the lateral surface (a thermally produced surface stress could show similar behavior). The negative step on the records coincides with the loading shock arrival and represents the rapid compression of the bar resulting from the shock passing directly over the strain gages. The lower record of S1 is the same S1 gage response at a faster recording speed and shows a smooth negative response of the bar, corresponding with the 4 μsec transit time of the shock over the

S1 gage width. Note the clean response of the bar to the shock loading and the absence of any associated overshoot and ringing. This response corresponds with the calculated response for the velocity conditions shown in Fig. 4(a). Figure 7 shows a similar record for strain gage output for a shock velocity ($V=1.79\times10^5$ cm/sec) greater than C_{min}. Oscillations follow the arrival of the shock as predicted by the theory, but they are damped because of the visco-elastic behavior of the Plexiglas.

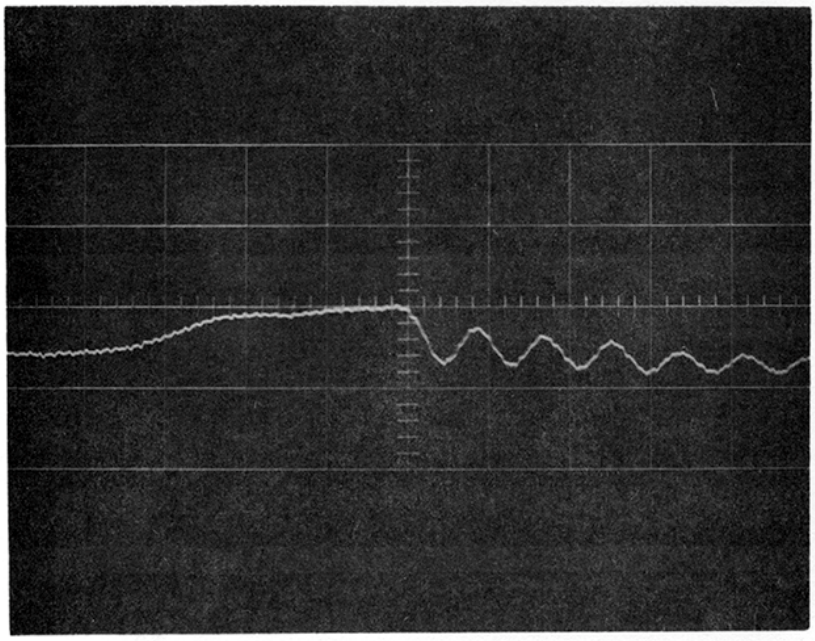

Fig. 7. S1 strain gage record for shock velocity $V=1.79\times10^5$ cm/sec [ref. 6].

5 Comparison of Experiment and Theory

Comparisons of experiment and theory were based on measurements taken from oscilloscope traces similar to those shown in Figs. 6 and 7, the measured shock velocity V, and the measured initial temperature and pressure of the gas. The pressure jump –P across the shock was calculated from normal shock tables[8] and the applied lateral surface stress $\tau_{zz}(z, a, t)$ was taken to be PS(t-z/V).

The experimental strain-time data were plotted along with the calculated strain histories. Only the strain wave traveling with the shock velocity is considered in this quantitative time-dependent strain comparison. Figures 8 and 9 show both calculated and experimental strain responses of the measuring bar to passage of the traveling air shock. The zero for the time coordinate used in the comparison occurs when the shock passes over the center of the strain gage. As data records did not contain an absolute indicator showing the arrival for the shock at the center of the gage, the experimental and calculated curves were aligned in time to obtain a best fit. The calculated strain data were averaged over a time interval τ corresponding to the transit time of the shock front across the width of the strain gage. This transit time in microseconds is indicated by a horizontal frag in each of Figs. 8 and 9. The possible data error in reducing the gage record to numerical data is shown by a vertical flag in each figure.

The values of the elastic bar parameters used in the calculations are

$C_s=1.27\times10^5$ cm/sec	shear velocity,
$C_o=2.08\times10^5$ cm/sec	bar velocity,
$C_d=2.64\times10^5$ cm/sec	dilatational velocity,
$\sigma= 0.35$	Poisson's ratio,
$E=5.22\times10^{10}$ dyn/cm^2	Young's modulus

The values were taken from Meitzler[9], whose measured values for the dilatational wave velocity in Plexiglas agreed within an experimental error of ±2% with ultrasonic measurements.

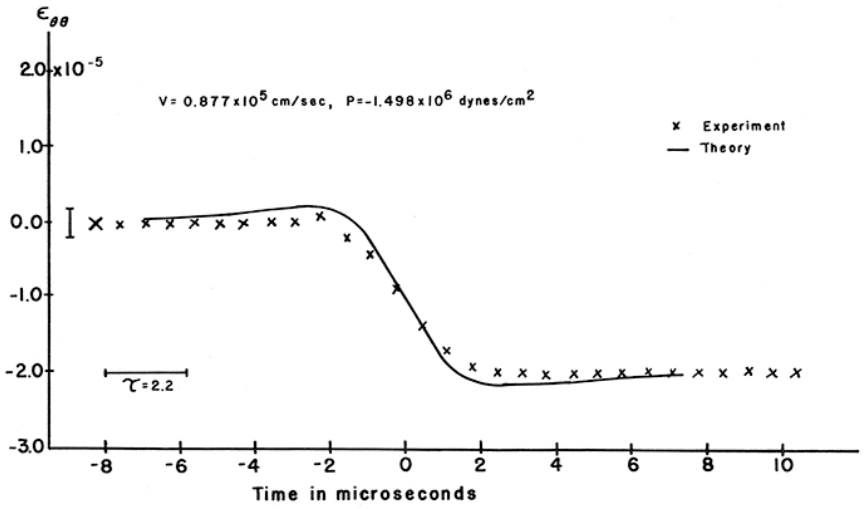

Fig. 8. Comparison of theory and experiment for strains produced by shock loading, V=0.887x10^5 cm/sec, P=-1.498x10^6 dyn/cm^2 [ref. 6].

Figure 8 shows the simple behavior of the bar typical of speeds V<¾C_s. The numerical data were taken from the S1 record in Fig. 6, converting the vertical scale from units of voltage to units of strain. The pressure jump across the shock front was 1.50x10^6 dyn/cm^2. A point-by-point comparison of experiment and theory in Fig. 8 shows the deviation of the two curves is less than the width of the oscilloscope trace. A correction for the high-frequency electrical response of the gage circuitry was not required.

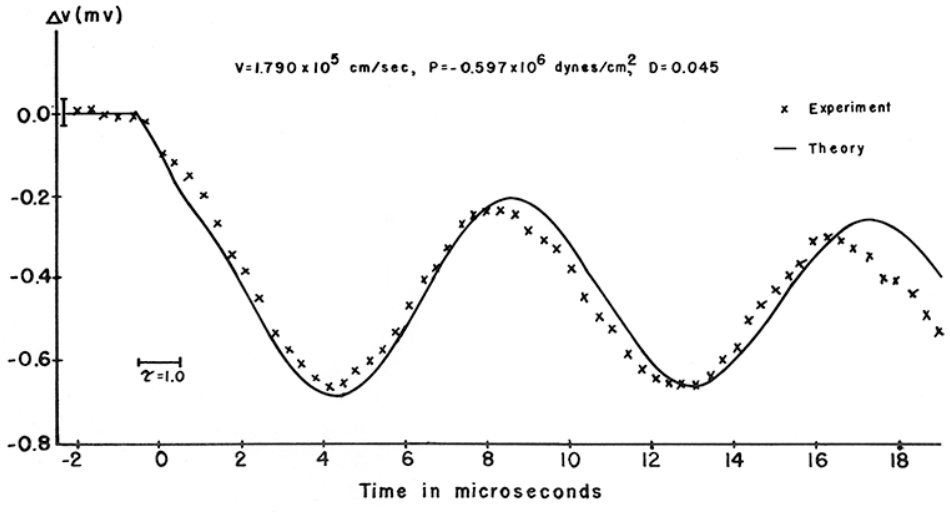

Fig. 9. Comparison of theory and experiment for strains produced by shock loading, V=1.79x10^5 cm/sec, P=-0.597x10^6 dyn/cm^2 [ref. 6].

Figure 9 compares experiment and theory in the higher velocity regime where oscillations follow shock arrival. While the agreement is good, there is a slight discrepancy between calculated and measured frequencies. It is noted that the PC oscillation frequency is determined by the intersection of the q=0 and q=1 mode in Fig. 3 and the slope of the curves is such that a small change in characteristic material velocities or shock velocity will result in a larger change in the intercept point and thus predicted oscillation frequency. An example of the sensitivity is seen in Fig. 10, which is a comparison of the same data in Fig. 9, but with the elastic parameters adjusted by 2%.

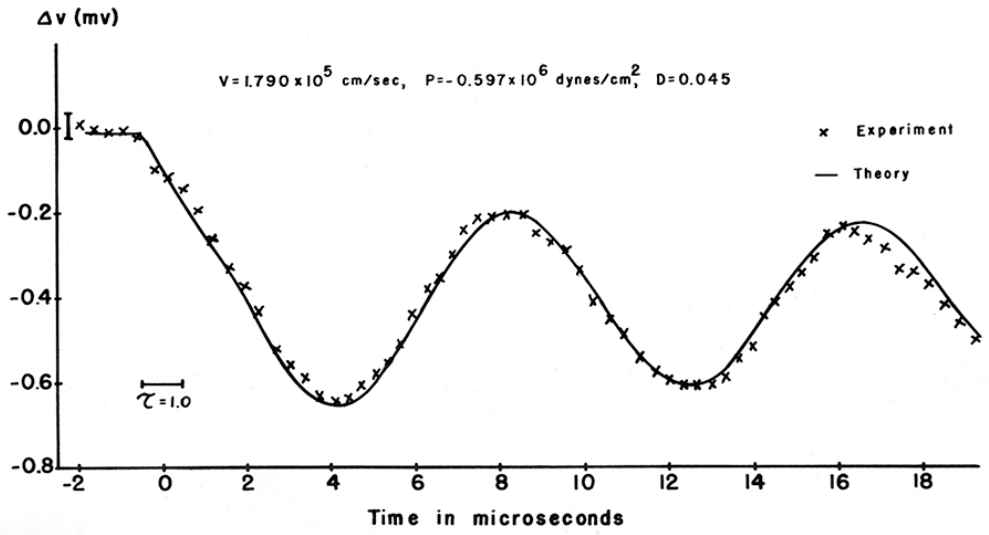

Fig. 10. Comparison of theory and experiment for strains produced by shock loading, V=1.79x10^5 cm/sec, P=-0.597x10^6 dyn/cm^2, adjusted parameters [ref. 6].

The improved agreement seen in Fig. 10 resulted from an increase in C_s, C_o, C_d of 2%. Note that values of these parameters were taken from Ref. 9 and were not independently measured for our bar material. With this small adjustment in parameters, the agreement with experiment is within the measurement error bars.

6 Summary

Prior work has been reviewed and referenced, which collectively provides a rigorous theoretical and experimental basis for realizing a non-dispersive response mode in a Hopkinson bar configuration. The configuration requires a lateral surface exposure to a shock loading pulse, which is consistent with

the pencil probe geometry and orientation for measurement of blast waves. To realize the non-dispersive behavior, the blast wave speed must be less than ¾ of the shear wave velocity of the bar material. In this lateral loading mode, the frequency response of the bar is not limited and thus the time resolution obtainable from the bar is determined by the strain sensor response and the transit time of the shock over the strain sensor in the bar. Additional considerations on bar design in addition to elastic parameters include material properties and surface finish to minimize effects of boundary layer drag and thermal conduction from shocked gas to the bar.

This collective of work demonstrates a capability through both theory and validating experiments for the direct utilization of a Hopkinson bar to faithfully reproduce a shock wave loading profile without the overshoot or ringing associated with the response of pressure transducers.

7 References

[1] Hopkinson, B.: Phil. Trans. R. Soc. Lond. A213 437-456 (1914).
[2] Pochhammer, L.: J. Math. (Crelle) **81**, 324 (1876).
[3] Chree, C.: J. Math. **21**, 287 (1886).
[4] Folk, R., Fox, G., Shook, C. A., and Curtis, C. W.: J. Acoust. Soc. Amer. **30**, 552-558 (1958).
[5] Baum, D. W.: J. Acoust. Soc. Amer. **52**, 5 (part 2), 1421-1428, (1972).
[6] Baum, D. W.: Thesis, Lehigh University, 1967.
[7] Values for the Airy function are tabulated by M. C. P. Miller, *The Airy Integral* (Cambridge University Press, New York, 1946).
[8] *Handbook of Supersonic Aerodynamics* (U. S. GPO, Washington, D. C., 1953.
[9] Meitzler, A. H.: Thesis, Lehigh University, 1955.

This work performed under the auspices of the U.S. Department of Energy by Lawrence Livermore National Laboratory under Contract DE-AC52-07NA27344.